Cannabidiol modulates PIEZO1 activity to regulate uterine contractility and pregnancy outcome.

Kun Cao[1, 5], Ruijia Lai[1, 5], Kaiyi Sun[2, 5], Qijing He[4], Mengya Cai[1], Jianmin Huang[1], Lu Gao[2]*, Bailong Xiao[4]*, Yang Zhang[1,3]*

1 Institute of Molecular Physiology, Shenzhen Bay Laboratory, Shenzhen, China

2 Department of Physiology, Naval Medical University, Shanghai, China

3 Shenzhen Medical Academy of Research and Translation, Shenzhen, China

4 School of Pharmaceutical Sciences, Tsinghua Medicine, Tsinghua University; Tsinghua-Peking Center for Life Sciences, Tsinghua University; IDG/McGovern Institute for Brain Research, Tsinghua University; State Key Laboratory of Membrane Biology, Tsinghua Medicine; New Cornerstone Science Laboratory, Tsinghua University; Beijing, 100084, China

5 These authors contributed equally to this work.

* Corresponding Author: Yang Zhang, Bailong Xiao, Lu Gao

Email: zhangyang@szbl.ac.cn

Author Contributions: Y.Z. conceived, designed, and supervised the project. K.C. performed the cell-based and animal experiments. R.L. conducted the electrophysiological studies. J.H. performed the Western blot analysis. L.G. and K.S. isolated and cultured primary cells. Q.H. and B.X. carried out calcium imaging experiments. Y.Z. and K.C. wrote the manuscript with input from all authors.

Competing Interest Statement: The authors declare no further competing interests.

Classification: Biological Sciences

Keywords: Preterm Birth, PIEZO1, Cannabidiol, Uterine Contractility

This PDF file includes:

Main Text
Figures 1 to 5

Abstract

Preterm birth is the leading cause of mortality in children under five worldwide. Aberrant uterine contractions, driven by calcium-dependent excitability of myometrial smooth muscle cells, are central to preterm labor. Current tocolytic agents target calcium signaling but pose cardiovascular risks to both mother and fetus. Here, we identify the mechanosensitive cation channel PIEZO1 as a key regulator of myometrial contractility. Activation of PIEZO1 elevates intracellular Ca^{2+} and triggers contraction in primary human myometrial smooth muscle cells and mouse uterine tissue. We further show that cannabidiol (CBD) acts as a potent PIEZO1 inhibitor, blocking Ca^{2+} influx and suppressing uterine contractions. In two mouse models of preterm birth, CBD markedly reduced myometrial contractility, delayed delivery, and improved fetal outcomes. These findings reveal an essential role for PIEZO1 in uterine contractility and highlight CBD-mediated PIEZO1 inhibition as a potential therapeutic strategy for preventing preterm labor.

Main Text

Introduction

Preterm birth stands as the leading cause of mortality in children under five years of age worldwide and remains a formidable global health challenge (1,2). The hallmark of this pathology is the premature onset of uterine contractions, a process driven by heightened myometrial excitability and tightly regulated by intracellular calcium homeostasis (3). Hormonal signaling via G protein-coupled receptors (GPCRs), such as oxytocin (4,5) and prostaglandins (6), promotes contraction by increasing intracellular calcium through sarcoplasmic reticulum release and store-operated calcium entry (3). A range of Ca^{2+}-permeable ion channels, including L-type, T-type voltage-gated Ca^{2+} channels as well as TRP channels, contribute directly to calcium influx and myometrial excitability (7–14). By contrast, Ca^{2+}-activated large-conductance potassium (BK) channels are activated by rising intracellular calcium, inducing potassium efflux and membrane repolarization, thereby closing calcium channels and serving as a negative feedback mechanism to relax the myometrium (15–17). During preterm labor, inflammatory mediators upregulate pro-contractile GPCRs and calcium channels, resulting in excessive Ca^{2+} increase and premature, sustained uterine contractions (18,19). Current tocolytic agents largely target calcium signaling to dampen myometrial activity, often limited by short duration of action and adverse maternal or fetal side effects (9,13,20,21). Consequently, there is an urgent need for effective strategies that target the upstream drivers of myometrial excitability.

Recent groundbreaking research has identified the mechanosensitive cation channels PIEZO as the essential transducers linking mechanical force to uterine contractility during parturition (22). Consistent with this emerging paradigm, we identify PIEZO1 (23–25) as a key regulator of myometrial contractility during pregnancy. PIEZO1 is functionally expressed in uterine smooth muscle, where its activation directly triggers contraction by elevating intracellular calcium levels. Both pharmacological inhibition and genetic ablation of PIEZO1 markedly suppress myometrial smooth muscle contractions driven by PIEZO1 agonists or oxytocin. Building on this mechanism, we investigated pharmacological interventions to target this pathway. We demonstrate that cannabidiol (CBD) acts as a potent inhibitor of uterine contraction by blocking PIEZO1-dependent calcium influx. In mouse models of preterm birth, CBD administration effectively delays delivery and improves pregnancy outcomes. Our findings not only corroborate the essential role of PIEZO1 in uterine biomechanics but also establish CBD-mediated PIEZO1 inhibition as a promising therapeutic strategy for preventing preterm birth.

Results

PIEZO1 mediates Ca^{2+} influx and contractile responses in myometrial smooth muscle.

Piezo channels are non-selective cation channels with high Ca^{2+} permeability that regulate mechanotransduction (25). qPCR analysis of myometrium revealed that PIEZO1 is the predominant Piezo channel in both human and mouse tissue (26,27). (Fig. 1*A* and SI Appendix, Fig. S1*A*). In mice, Piezo1 expression was reduced during gestation compared with that in non-pregnant controls (SI Appendix, Fig. S1*B*). At term labor, however, Piezo1 levels were markedly upregulated, highlighting its potential role in parturition (SI Appendix, Fig. S1*B*). Immunofluorescence confirmed that PIEZO1 localizes to the plasma membrane of primary human myometrial smooth muscle cells (HUSMCs), confirmed by α-SMC-actin staining (Fig. 1*B* and SI Appendix, Fig. S1*C*). Pressure clamp electrophysiology recording elicited a mechanosensitive current from HUSMCs with a unitary conductance of 28.49 ± 2.18 pS (Fig. 1*C*-*D*) (28), which aligns with the typical single channel conductance of PIEZO1. Whole-cell patch-clamp recordings detected probe-induced PIEZO1 currents in HUSMCs, which were abolished by the PIEZO1 inhibitor GsMTx4 (Fig. 1*E*-*F*). Yoda1, a PIEZO1 agonist, robustly increased intracellular Ca^{2+}, which was suppressed by GsMTx4 but unaffected by Ionomycin treatment (Fig. 1*G*). Correspondingly, Yoda1 induced contraction of HUSMCs-embedded collagen gels, which was prevented by GsMTx4

(Fig. 1*H*). In ex vivo uterine strips from wild-type mice, Yoda1 similarly enhanced contractility (SI Appendix, Fig. S1*E*-*G*), which was suppressed by ruthenium red. These results establish PIEZO1 as a functional mechanotransducer linking mechanical stimuli to Ca^{2+} entry and myometrial contraction.

Cannabidiol suppresses PIEZO1-dependent Ca^{2+} entry in myometrial smooth muscle.

Pharmacological inhibition of PIEZO1 could suppress Ca^{2+} influx in HUSMCs, thereby reducing uterine contractions in preterm labor. To identify pregnancy-safe inhibitors of PIEZO1, we screened small molecules and found cannabidiol (CBD) to be a potent inhibitor of PIEZO1 channel activity. To directly assess its effect on PIEZO1 activity, we performed patch-clamp electrophysiology on hPIEZO1 overexpressed HEK293T cells. Pressure-clamp recordings showed that 20 μM CBD significantly reduced the open probability of the PIEZO1 channel without affecting the conductance (Fig. 2*A*-*B*). Whole-cell patch-clamp recordings revealed that CBD inhibited PIEZO1 currents in a concentration-dependent manner, with a half-maximal inhibitory concentration (IC50) of 9.414 μM (Fig. 2*C*-*D*). Similar suppression was observed in primary HUSMCs, indicating that CBD targets the endogenous PIEZO1 channel (Fig. 2*E*-*H*). These data provide direct electrophysiological evidence that CBD is a potent PIEZO1 inhibitor.

Consistent with these findings, 10 μM CBD completely abolished Yoda1-induced Ca^{2+} influx in Piezo1 overexpressing HEK293T cells (Fig. 3*A*-*B*) and in primary HUSMCs (Fig. 3*C*). PIEZO1-deficient HUSMCs failed to respond to Yoda1, while ionomycin-induced Ca^{2+} elevation remained intact, confirming specificity (Fig. 3*C*-*D* and SI Appendix, Fig. S1*D*). At the tissue level, two-photon calcium imaging further confirmed that Yoda1 markedly increased Ca^{2+} entry in isolated mouse uterine smooth muscle tissue, which was significantly suppressed by co-treatment with CBD (Fig. 3*E*-*F*). Together, these findings demonstrate that CBD effectively inhibits PIEZO1-mediated Ca^{2+} influx in both cells and tissues, which could limit uterine smooth muscle excitability and contraction.

CBD inhibits PIEZO1-dependent uterine contraction.

Activation of PIEZO1 elevates intracellular Ca^{2+} levels, thereby driving uterine smooth muscle contraction. Because CBD inhibits PIEZO1-mediated Ca^{2+} influx in both myometrial smooth muscle cells (mSMCs) and intact myometrial tissue, we next examined whether CBD influences myometrial contractility. In collagen gel assays containing HUSMCs, CBD potently suppressed Yoda1-induced contraction, phenocopying the effect of PIEZO1 deletion (Fig. 4*A*-*B*). Similar inhibition was observed in ex vivo uterine strips from WT mice, where CBD effectively abolished Yoda1-evoked contractions (Fig. 4*C*-*D* and SI Appendix, Fig. S3*A*-*D*). Isometric tension recordings showed that co-application of 20 mM tetraethylammonium chloride (TEA) and Yoda1 enhanced mean contraction amplitude (from 1.036± 0.278 g to 1.333 ± 0.295 g) and frequency (from 0.128 ± 0.037 Hz to 0.257 ± 0.108 Hz), whereas subsequent 5 μM CBD treatment markedly reversed these effects, reducing amplitude to 0.777 ± 0.339 g and frequency to 0.163 ± 0.064 Hz.

We next examined whether CBD also affects oxytocin-induced contractions, as oxytocin is the principal hormonal driver of myometrial activity during labor. CBD significantly attenuated oxytocin-induced gel contraction, mirroring the effect of PIEZO1 ablation (Fig. 4*E*-*F*). In isolated uterine strips, 2 nM oxytocin increased mean contraction amplitude (from 0.318 ± 0.127 g to 0.602 ± 0.074 g) and frequency (from 0.045 ± 0.017 Hz to 0.065 ± 0.011 Hz), both of which were restored to baseline by 5 μM CBD treatment (mean amplitude 0.100 ± 0.074 g; frequency 0.027 ± 0.007 Hz; Fig. 4*G*-*H*). This inhibition was dose-dependent and comparable to that of benzbromarone, a known PIEZO1 blocker (SI Appendix, Fig. S2*A*-*B*, S3*E*-*F*). Importantly, CBD did not alter oxytocin-evoked Ca2+ transients (SI Appendix, Fig. S2*C*-*D*), indicating that it suppresses contraction independently of oxytocin receptor signaling.

Thus, CBD inhibits both PIEZO1- and oxytocin-driven uterine contractions, revealing its potential as a modulator of myometrial excitability.

CBD delays preterm labor and improves pregnancy outcomes.

To evaluate the therapeutic potential of CBD in vivo, we employed LPS- and RU486-induced mouse models of preterm birth (SI Appendix, Fig. S4*A*) (29). Notably, both stimuli markedly increased PIEZO1 expression in myometrium at labor onset, as revealed by qPCR and immunoblotting (Fig. 5*A*-*D*). Consistently, uterine contractility was enhanced in both models: contraction frequency increased from 0.033 ± 0.002 Hz in control mice to 0.044 ± 0.003 Hz and

0.050 ± 0.0003 Hz in LPS- and RU486-treated mice, respectively. These increases were significantly reduced by 5 μM CBD (Fig. 5*E*). When exposed to 2 nM oxytocin, uterine strips from LPS- and RU486-treated mice exhibited elevated mean contraction forces (from 0.463 ± 0.078 g to 0.938 ± 0.215 g, and from 0.603 ± 0.082 g to 1.195 ± 0.066 g, respectively), both of which were effectively suppressed by CBD (Fig. 5*E*-*G*). These data identify CBD as a potent inhibitor of pathological uterine hypercontractility.

In the LPS-induced preterm birth model, control mice delivered 15.33 ± 1.52 h after LPS injection, whereas nifedipine, a clinically used tocolytic agent (9), extended the delivery interval to 41.81 ± 6.88 h. Remarkably, CBD (20 mg/kg) prolonged delivery to 61.60 ± 4.95 h (Fig. 5*H*). Both nifedipine and CBD treatment improved the pup's body weight, indicating enhanced fetal development.

In the RU486 model, the control and nifedipine groups showed similar delivery times (17.50 ± 0.57 h and 17.40 ± 0.37 h, respectively), whereas CBD (30 mg /kg) delayed birth to 24.94 ± 2.54 h (Fig. 5*I*), with comparable pup weights across groups.

Collectively, these findings demonstrate that CBD suppresses pathological uterine hypercontractility via PIEZO1 inhibition, prolonging gestation and improving fetal outcomes in preterm birth models. This work identifies PIEZO1 blockade by CBD as a promising therapeutic strategy for the prevention of preterm labor.

Discussion

Our study identifies the mechanosensitive ion channel PIEZO1 as a critical regulator of uterine contractility and reveals CBD as a potent pharmacological inhibitor capable of modulating this pathway. We demonstrate that PIEZO1 activation elevates intracellular Ca^{2+} to drive myometrial excitation and contraction, whereas CBD suppresses both calcium influx and pathological hypercontractility, thereby significantly prolonging gestation in preterm birth models. These findings expand the physiological repertoire of PIEZO1 beyond its established functions in vascular, epithelial, placental, and erythrocyte mechanotransduction, positioning it as a key determinant of uterine biomechanics during pregnancy.

PIEZO1 expression dynamically changes across gestation: it is downregulated during mid-pregnancy but markedly upregulated at term labor (22,26,27). Similarly, in LPS- and RU486-induced preterm birth models, PIEZO1 expression in the myometrium is robustly elevated. This upregulation under both physiological and pathological contexts suggests that mechanical and inflammatory cues converge on PIEZO1 to amplify contractile signaling. Such regulation likely reflects the opposing demands for uterine quiescence during pregnancy and strong contractility at labor onset (22). Supporting this notion, we observed that MyoD-family inhibitor proteins MDFIC and MDFI, recently identified as auxiliary subunits that slow PIEZO1 inactivation and prolong calcium entry (30), were also increased in LPS- and RU486-treated myometrium (SI Appendix, Fig. S4B). By blocking PIEZO1-dependent calcium influx, CBD provides an effective and well-tolerated means to restore myometrial quiescence under pro-contractile stress.

Mechanistically, CBD selectively inhibits PIEZO1-dependent Ca^{2+} entry without affecting oxytocin-evoked Ca^{2+} transients in HUSMCs (Fig. 3*C*- *D* and SI Appendix, Fig S2*C*-*D*), yet it suppresses both PIEZO1- and oxytocin-induced contractions (Fig 4). We propose that oxytocin receptor activation initiates transient calcium increases that trigger contraction, which in turn mechanically activates PIEZO1 to further amplify Ca^{2+} entry and sustain contractile activity. Inhibition of PIEZO1 by CBD would thus interrupt this positive feedback loop, attenuating the amplification phase of oxytocin-driven contractions and contributing to the observed prolongation of gestation in preterm birth models.

Several PIEZO1 inhibitors have been reported, including the non-specific mechanosensitive channel blockers GsMTx4, ruthenium red, and gadolinium ions (Gd^{3+}) (24). However, their lack of specificity and poor pharmacological profiles preclude clinical application. Benzbromarone, an anti-gout agent identified as a PIEZO1 inhibitor that alleviates hereditary xerocytosis (31), is contraindicated in pregnancy due to hepatic and renal toxicity risks. By contrast, CBD, a phytocannabinoid broadly used for pain management, epilepsy, and inflammatory disorders, exerts

rapid, reversible inhibition of PIEZO1 with a favorable safety profile (32,33). Although further studies are needed to evaluate its pharmacokinetics and safety in pregnancy, CBD emerges as a compelling lead compound for the development of PIEZO1-targeted tocolytics.

In summary, our work identifies PIEZO1 as a pivotal mechanotransducer controlling uterine excitability and establishes CBD-mediated PIEZO1 inhibition as a novel and effective strategy to prevent aberrant uterine contractions and preterm labor. These findings not only elucidate a fundamental mechanism underlying uterine biomechanics but also open therapeutic avenues for targeting mechanosensitive calcium entry in pregnancy-associated and other uterine SMC disorders, including dysmenorrhea.

Materials and Methods

Cell lines

HEK293T cells (gift from Dr. Tingting Chu, Shenzhen Bay Laboratory) were maintained in Dulbecco's Modified Eagle Medium (DMEM) (11995-065, Gibco) supplemented with 10% (v/v) fetal bovine serum (F2442, Sigma-Aldrich) and 1% (v/v) penicillin-streptomycin (15-140-122, Gibco) at 37°C in a humidified atmosphere containing 5% CO_2.

Primary cells isolation and culture

Human uterine tissue collection was performed under institutional ethics approval (20210308002, Naval Medical University Ethics Committee). Fresh specimens were immediately rinsed in phosphate-buffered saline (PBS) (C10010500BT, Gibco) to remove residual blood and transported on ice in pre-chilled Hank's Balanced Salt Solution (HBSS) (14025092, Gibco). Under sterile conditions, tissues were microscopically dissected to isolate endometrial and myometrial layers, with careful removal of vascular components. Myometrial tissue was minced to ~1 mm^3 fragments and enzymatically digested in HBSS containing 0.1% collagenase B (11088807001, Roche) and antibiotic solution for 1 h at 37°C with gentle agitation every 15 min. Digested tissue was filtered through 70-μm cell strainers and centrifuged at 900 rpm for 10 min. Cell pellets were resuspended in Dulbecco's Modified Eagle Medium (11995-065, Gibco) supplemented with 10% fetal bovine serum and 0.2% penicillin/streptomycin (15-140-122, Gibco).

Primary myometrial smooth muscle cells were enriched using differential adhesion: cell suspensions were initially plated on non-treated plastic dishes for 1 h to allow preferential attachment of smooth muscle cells. Non-adherent cells were subsequently transferred to standard 6-cm culture dishes and maintained at 37°C in 5% CO_2. Medium was replaced after 24 h, and cells were subcultured upon reaching 60-70% confluence. Passage 3 cells were used for all experiments.

Whole-cell patch-clamp

Whole-cell patch-clamp recordings were performed at room temperature (22–24 °C). Briefly, patch pipettes were prepared from borosilicate glass capillaries (BF150-86-10, Sutter Instrument) using a P-97 pipette puller (Sutter Instrument) and had a resistance of 3.0–6.0 MΩ. After forming GΩ-resistance seals, the whole-cell configuration was established. All electrophysiology recordings were performed with an Axopatch 200B amplifier (Molecular Devices) and pClamp 11.2. Currents were filtered at 10 kHz using a low-pass Bessel filter of the amplifier and digitized using a Digitata 1550B (Molecular Devices). All voltage-clamp measurements were performed at a holding voltage of −60 mV. All measurements were performed using an extracellular solution containing 140 mM CsCl, 1 mM $MgCl_2$, 2.5 mM $CaCl_2$,10 mM HEPES (pH adjusted to 7.4 with CsOH). The patch pipette solution for voltage-clamp measurements contained 140 mM CsCl, 1 mM $MgCl_2$, 10 mM HEPES (pH adjusted to 7.4 with CsOH). Mechanically activated currents were measured from HEK 293T and SMC cells. Briefly, mechanical stimulation was performed using a heat-polished glass pipette (tip diameter about 3 μm) controlled by K-Cube Combined Piezo Controller (KPC101, Thorlabs) positioned at 60° to the surface of the cover glass. Cells received a membrane indentation lasting 300 ms at a depth of 4.0 Δ + 0.5 μm/5 s. For the drug stimulation experiments, during the recording of Piezo1 currents in HEK 293T cells, different concentrations of CBD (13956-29-1, zzstandard) were directly added to the bath solution. In SMC recordings of mechanically

activated currents, 20 μM CBD (13956-29-1, zzstandard) or 1 μM GsMTx4 (HY-P1410, MedChemExpress) was directly added to the bath solution.

Single-Channel Recordings

All single-channel currents were recorded in the cell-attach configuration using an Axopatch 200B amplifier (Molecular Devices) and the pClamp 11.2 software package (Molecular Devices). Glass pipettes were pulled from borosilicate capillaries (Sutter Instruments) and fire-polished using a microforge (Narishige) with a resistance of 7-10 MΩ for single-channel recordings. The bath solution consisted of the following (in mM): 140 CsCl, 10 HEPES, and 1 $MgCl_2$, with the pH adjusted to 7.4 using CsOH. The pipette solution contained (in mM): 140 CsCl, 10 HEPES, and 1 $MgCl_2$, with the pH adjusted to 7.4 using CsOH. For CBD (13956-29-1, zzstandard) treatment experiments, 20 μM CBD was added to the pipette solution to record single-channel currents. PIEZO1 activation was achieved by applying pressure using a high-speed pressure clamp (HSPC-2-SB, ALA Scientific Instruments). The patch resistance increased to 10 GΩ after the pipette formed a tight seal with the cell membrane. All data were acquired at 20 kHz with a 2 kHz low-pass filter.

Spontaneous movement of the isolated mouse uterus

Mice were anesthetized with isoflurane (26675-46-7, RWD), and their abdomens were fixed upward on the operating table. After disinfection, the abdominal skin and peritoneum were carefully incised using tissue scissors, and the abdominal cavity was exposed to remove any excess tissue. The uterus and its adnexa were then carefully isolated from the vagina, washed with PBS (C10010500BT, Gibco), and placed in a thermostatic smooth muscle test system. This system was supplemented with 20 ml of oxygenated Krebs-Ringer solution (composition of storage solution for 1000 ml: calcium chloride dihydrate 7.35 g, potassium chloride 7.01 g, magnesium chloride hexahydrate 4.88 g, sodium dihydrogen phosphate 3.74 g; composition of Krebs-Ringer solution for 2000 ml: sodium chloride 13.67 g, sodium bicarbonate 4.20 g, glucose 3.96 g, storage solution 100 ml, pH adjusted to 7.4). The BF-420N system was employed to record stable uterine spontaneous contraction force for 20 minutes. Subsequently, drugs such as 2 nM oxytocin (HY-P4605A, MedChemExpress), 3 μM Yoda1 (21904, Cayman), and cannabidiol (CBD) (13956-29-1, zzstandard) were introduced, and the uterine spontaneous contraction was observed for an additional 20 minutes. Data analysis was performed using MATLAB software.

Calcium imaging of the isolated mouse uterus

Adult female rats were anesthetized with isoflurane and positioned on the operating table. Uterine tissues were carefully excised and processed as described previously. The uterus was washed and then dissected under a body microscope (Zeiss Stemi 508). The endometrium was scraped off, and the tissue was placed on a plate containing HBSS (14025092, Gibco) with 2 μM Calbryte 520 AM Ca^{2+} dye (20651, AAT Bioquest) and 10% Pluronic F-127 (P2443-250G, Sigma-Aldrich). The preparation was incubated for 1 hour at 37°C in a CO_2 incubator. Time-lapse calcium imaging was performed using a multiphoton laser scanning microscope. Changes in calcium signal intensity were analyzed using ImageJ and MATLAB software.

Collagen Gel Contraction Assay

Primary myometrial smooth muscle cells were harvested and resuspended in complete DMEM culture medium. A type I collagen solution (C8062-10mg, Solarbio) was neutralized on ice according to the manufacturer's instructions using neutralization buffer (0.1 M NaOH and 10x DMEM). The cell suspension was then mixed with the neutralized collagen solution to achieve a final density of 2.5 x 10^5 cells/mL in a collagen concentration of 1.5 mg/mL. Aliquots of 500 μL of the cell-collagen mixture were carefully pipetted into each well of a 24-well plate that had been pre-coated with 2% bovine serum albumin (BSA) (9048-46-8, Sigma-Aldrich) to prevent gel adhesion. The plate was incubated at 37°C for 1 hour to allow for complete collagen polymerization.

Following polymerization, the gels were gently released from the walls and bottom of the wells using a sterile pipette tip. Fresh serum-free medium, containing the designated treatments, was then carefully added to each well. The gels were allowed to contract for 24 hours at 37°C. Contraction was quantified by capturing digital images of the gels at the indicated time points. The gel area was measured using ImageJ software and expressed as a percentage of the initial area (time 0). Each condition was performed in at least triplicate.

Western blot

Cells or tissues were lysed on ice using RIPA lysis buffer (89900, Thermo Scientific) supplemented with a complete protease and phosphatase inhibitor cocktail (87786, Thermo Scientific). The lysates were centrifuged at 13000 rpm for 15 minutes at 4°C, and the supernatants were collected. Protein concentration was determined using a Nanodrop device. Proteins (20 μg) were mixed with 5× SDS-PAGE Protein Loading Buffer (20315ES05, YEASEN), separated on a 4-20% polyacrylamide gel (36270ES10, YEASEN). The separated proteins were electrophoretically transferred onto a PVDF membrane (IPVH00010, Merck Millipore). The membrane was then blocked with 5% non-fat milk in Tris-buffered saline containing 0.1% Tween-20(9005-64-5, Sigma-Aldrich) (TBST) for 1 hour at room temperature. The following primary antibody, Piezo1 (extracellular domain) recombinant antibody (15939-1-AP, 1:1000, Proteintech) was used. After washing three times with TBST, the membrane was incubated with the HRP-linked anti-rabbit IgG secondary antibody (A0545, 1:10000, Sigma-Aldrich) for 1 hour at room temperature. Protein bands were visualized using an enhanced chemiluminescence (ECL) substrate (E423-01, Vazyme) and imaged with a ChemiDoc MP Imaging System (Bio-Rad). Band intensities were quantified using ImageJ software. The expression level of the target protein was normalized to that of GAPDH as a loading control.

Immunofluorescence staining

Cells cultured in monolayers were fixed with 4% paraformaldehyde (4% PFA, E672002-0500, BBI), permeabilized using 0.2% Triton X-100 (93443-100ML, Sigma-Aldrich), and blocked with 10% goat serum (16210072, Gibco) following antibody staining. The specific primary antibody, Piezo1 (extracellular domain) recombinant antibody (15939-1-AP, Proteintech), was incubated overnight. Fluorescent labeling was carried out with Alexa Fluor 488 (35552, Molecular Probes). The slides were counterstained with Hoechst 33342 (H3570, Invitrogen, 1:1000) for 5 minutes and then sealed. Fluorescence images were acquired using a Zeiss LSM 980 inverted confocal microscope. Image analysis was performed using ZEN 3.6 and ImageJ-win64 software.

Fluorescence imaging of Ca^{2+}

To monitor Ca^{2+} dynamics, cells were incubated with 0.5–1 μM Calbryte 590 AM Ca^{2+} dye (20701, AAT Bioquest) for 10 to 20 minutes at 37 °C. Yoda1 was then applied to activate Piezo1 channels. Ca^{2+} dynamics were recorded using a Zeiss LSM 980 inverted confocal microscope at 5-second intervals over 140 cycles. Data analysis was conducted using ZEN 3.6 and MATLAB.

Mice studies and ethics statement

All procedures involving mice were executed in strict accordance with the ethics of laboratory animals in Shenzhen Bay Laboratory (Ethics No. AEZYANG202301). Mice of the C57BL/6 strain were maintained in specific pathogen-free conditions at the Second Military Medical University and housed in open cages at 25 ± 1 °C under a constant 12 h light-dark cycle regimen, with ad libitum access to standard rodent food and water.

Normal pregnancy and term labor

To generate pregnant mice, virgin female C57BL/6 outbred mice, aged 8-10 weeks, were mated with wild-type male overnight beginning at 18:00. The presence of a copulatory plug at 08:00 the following day was considered to be 0.5 days post coitum, with term labor occurring usually at the 19.5 dpc. Pregnant females were euthanized after delivery of the first pup on 19.5 dpc.

Mice models for preterm labor

RU486-induced preterm labor: On day 15.5 of gestation, two groups of mice were treated with either RU486 (S2606, Selleck), 150μg, subcutaneous injection, at 5:00 p.m., a concentration of 50 mM in DMSO or with vehicle (6.9 μL DMSO) as described previously. The mice were closely observed for the onset of labor, as indicated by the delivery of at least one pup.

LPS-induced preterm labor: On day 16.5 of gestation, two groups of mice were treated with either LPS (L2880, Sigma-Aldrich) at 5:00 p.m. at 100 μg/kg, subcutaneous injection at 5:00 p.m., in 1 mg/ml water. The mice were closely observed for the onset of labor, as indicated by the delivery of at least one pup.

Statistical analysis

Statistical analyses were performed using Prism 10 (GraphPad) for Windows. The two groups were compared using Student's *t*-test and Two-way ANOVA. $*P < 0.05$, $**P < 0.01$, $***P < 0.001$, and

****$P < 0.0001$ were considered significant, and $P > 0.05$ was considered not significant (ns). Details of statistical analyses and biological replicates are described in each figure legend.

Acknowledgments

This work was supported by Shenzhen Medical Research Fund B2502023, the National Natural Science Foundation of China grant 32300603, and Guangdong Pearl River Program 2023QN10Y164.

References

1. Perin, J. et al. Global, regional, and national causes of under-5 mortality in 2000–19: an updated systematic analysis with implications for the Sustainable Development Goals. Lancet Child Adolesc. Health 6, 106–115 (2022).
2. Ohuma, E. O. et al. National, regional, and global estimates of preterm birth in 2020, with trends from 2010: a systematic analysis. The Lancet 402, 1261–1271 (2023).
3. Malik, M., Roh, M. & England, S. K. Uterine contractions in rodent models and humans. Acta Physiol. Oxf. Engl. 231, e13607 (2021).
4. Flenady, V., Reinebrant, H. E., Liley, H. G., Tambimuttu, E. G. & Papatsonis, D. N. Oxytocin receptor antagonists for inhibiting preterm labour. Cochrane Database Syst. Rev. https://doi.org/10.1002/14651858.CD004452.pub3(2014),doi:10.1002/14651858.CD004452.pub3.
5. Jurek, B. & Neumann, I. D. The Oxytocin Receptor: From Intracellular Signaling to Behavior. Physiol. Rev. 98, 1805–1908 (2018).
6. Myatt, L. & Lye, S. J. Expression, localization and function of prostaglandin receptors in myometrium. Prostaglandins Leukot. Essent. Fatty Acids 70, 137–148 (2004).
7. Wray, S. Insights into the uterus. Exp. Physiol. 92, 621–631 (2007).
8. Wray, S. & Arrowsmith, S. Uterine Excitability and Ion Channels and Their Changes with Gestation and Hormonal Environment. Annu. Rev. Physiol. 83, 331–357 (2021).
9. Flenady, V. et al. Calcium channel blockers for inhibiting preterm labour and birth. Cochrane Database Syst. Rev. 2014, CD002255 (2014).
10. Ohkubo, T., Kawarabayashi, T., Inoue, Y. & Kitamura, K. Differential Expression of L- and T-Type Calcium Channels between Longitudinal and Circular Muscles of the Rat Myometrium during Pregnancy. Gynecol. Obstet. Invest. 59, 80–85 (2005).
11. Villegas, D., Giard, O., Brochu-Gaudreau, K. & Rousseau, É. Activation of TRPV4 channels leads to a consistent tocolytic effect on human myometrial tissues. Eur. J. Obstet. Gynecol. Reprod. Biol. X 10, 100124 (2021).
12. Ying, L. et al. The transient receptor potential vanilloid 4 channel modulates uterine tone during pregnancy. Sci. Transl. Med. 7, 319ra204-319ra204 (2015).
13. Senadheera, S. et al. Enhanced contractility in pregnancy is associated with augmented TRPC3, L-type, and T-type voltage-dependent calcium channel function in rat uterine radial artery. Am. J. Physiol.-Regul. Integr. Comp. Physiol. 305, R917–R926 (2013).
14. Jing, C. et al. TRPC3 Overexpression Promotes the Progression of Inflammation-Induced Preterm Labor and Inhibits T Cell Activation. Cell. Physiol. Biochem. 45, 378–388 (2018).
15. Wakle-Prabagaran, M. et al. BK Ca channel regulates calcium oscillations induced by alpha-2-macroglobulin in human myometrial smooth muscle cells. Proc. Natl. Acad. Sci. 113, (2016).
16. Li, Y., Lorca, R. A., Ma, X., Rhodes, A. & England, S. K. BK Channels Regulate Myometrial Contraction by Modulating Nuclear Translocation of NF-κB. Endocrinology 155, 3112–3122 (2014).
17. Kent, L. N. et al. Blocking the BKCa channel induces NF-κB nuclear translocation by increasing nuclear calcium concentration†. Biol. Reprod. 106, 441–448 (2021).

18. Habelrih, T. et al. Inflammatory mechanisms of preterm labor and emerging anti-inflammatory interventions. Cytokine Growth Factor Rev. 78, 50–63 (2024).
19. Kwame, A.-B. & Fidelis, B. Pathophysiological mechanisms of maternal pro-inflammatory mediators in preterm labour. J. Physiol. Pathophysiol. 13, 1–16 (2022).
20. Arman, B. M. et al. Assessment of the tocolytic nifedipine in preclinical primary models of preterm birth. Sci. Rep. 13, 5646 (2023).
21. Siricilla, S. et al. Arrest of mouse preterm labor until term delivery by combination therapy with atosiban and mundulone, a natural product with tocolytic efficacy. Pharmacol. Res. 195, 106876 (2023).
22. Zhang, Y. et al. PIEZO channels link mechanical forces to uterine contractions in parturition. Science 390, eady3045 (2025).
23. Zhang, Y. et al. Mechanosensitive Piezo1 channel: an emerging target in demyelination disease. Front. Cell. Neurosci. 19, (2025).
24. Thien, N. D., Hai-Nam, N., Anh, D. T. & Baecker, D. Piezo1 and its inhibitors: Overview and perspectives. Eur. J. Med. Chem. 273, 116502 (2024).
25. Xiao, B. Mechanisms of mechanotransduction and physiological roles of PIEZO channels. Nat. Rev. Mol. Cell Biol. 25, 886–903 (2024).
26. Barnett, S. D., Asif, H. & Buxton, I. L. O. Novel identification and modulation of the mechanosensitive Piezo1 channel in human myometrium. J. Physiol. 601, 1675–1690 (2023).
27. Bi, Y. et al. Piezo1 overexpression in the uterus contributes to myometrium contraction and inflammation-associated preterm birth. J. Transl. Med. 22, 1140 (2024).
28. Zhang, Y. et al. PIEZO1 drives trophoblast fusion and placental development. Nat. Commun. 16, 6895 (2025).
29. McCarthy, R. et al. Mouse models of preterm birth: suggested assessment and reporting guidelines. Biol. Reprod. 99, 922–937 (2018).
30. Zhou, Z. et al. MyoD-family inhibitor proteins act as auxiliary subunits of Piezo channels. Science 381, 799–804 (2023).
31. Liang, P. et al. Deciphering and disrupting PIEZO1-TMEM16F interplay in hereditary xerocytosis. Blood 143, 357–369 (2024).
32. García-Gutiérrez, M. S. et al. Cannabidiol: A Potential New Alternative for the Treatment of Anxiety, Depression, and Psychotic Disorders. Biomolecules 10, 1575 (2020).
33. Britch, S. C., Babalonis, S. & Walsh, S. L. Cannabidiol: Pharmacology and Therapeutic Targets. Psychopharmacology (Berl.) 238, 9–28 (2021).

Figure 1

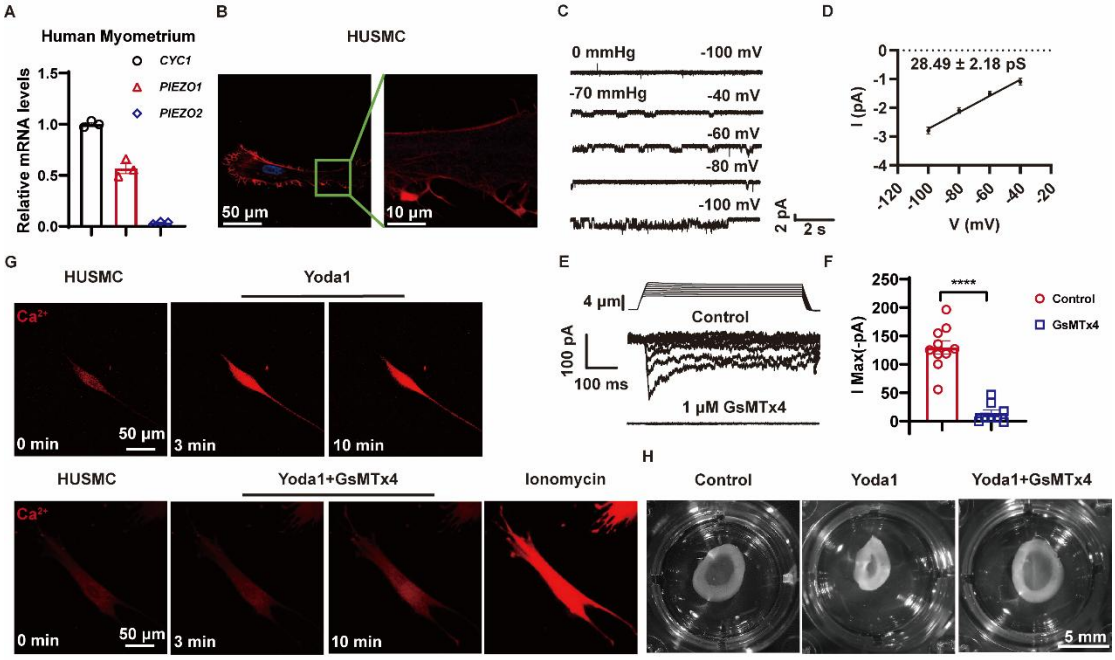

Fig. 1. Piezo1 is functionally expressed in the myometrium. (*A*), PIEZO1 and PIEZO2 mRNA expression measured via RT-qPCR in the human myometrium. All gene expression levels were normalized to *GAPDH*, and subsequently to Cytochrome C1 (*CYC1*). (*n* = 3 from three patients). (*B*), Immunofluorescence of PIEZO1 (red) in primary human myometrial smooth muscle cells (HUSMCs) and counterstained with a nuclear marker (blue). Images are representative of three experiments. Scale bar, 50 μm (left), 10 μm (Right). (*C*), The single-channel recordings of PIEZO1 in response to a -70 mmHg pressure pulse at various membrane potentials. Membrane potential was stepped from -100 mV to -40 mV in 20 mV increments from a holding potential of -60 mV. (*D*), Current-voltage (I-V) plot of the single-channel currents shown in (*C*). The single-channel conductance is 28.49 ± 2.18 pS, as determined by linear regression (*n* = 7 cells). (*E*), The whole-cell patch-clamp recordings from HUSMCs before (Control) and after application of the PIEZO1 inhibitor GsMTx4 (1 μM). Mechanical stimulation (4.0 ± 0.5 μm indentation for 300 ms) was delivered from a holding potential of -80 mV. GsMTx4 inhibits mechanically-activated currents in HUSMCs. (*F*), Quantification of peak current amplitude (I_{max}) for control and GsMTx4-treated cells. (Control group *n* = 10; GsMTx4 group *n* = 8; ****$P < 0.0001$; Students unpaired *t*-test; mean ± SEM). (*G*), The PIEZO1 agonist Yoda1 (5 μM) triggers robust intracellular Ca^{2+} elevation in HUSMCs. The PIEZO1 antagonist GsMTx4 (5 μM) abolishes Yoda1-induced Ca^{2+} influx in HUSMCs. Ca^{2+} elevation by ionomycin remains intact in the presence of GsMTx4. All traces/images in (*G*) are representative of at least three independent experiments. (*H*), Representative images of collagen gel contraction assays in HUSMCs treated with the PIEZO1 agonist Yoda1 (5 μM), with or without the antagonist GsMTx4 (5 μM). GsMTx4 inhibits gel contraction. Images are representative of at least three biological replicates.

Figure 2

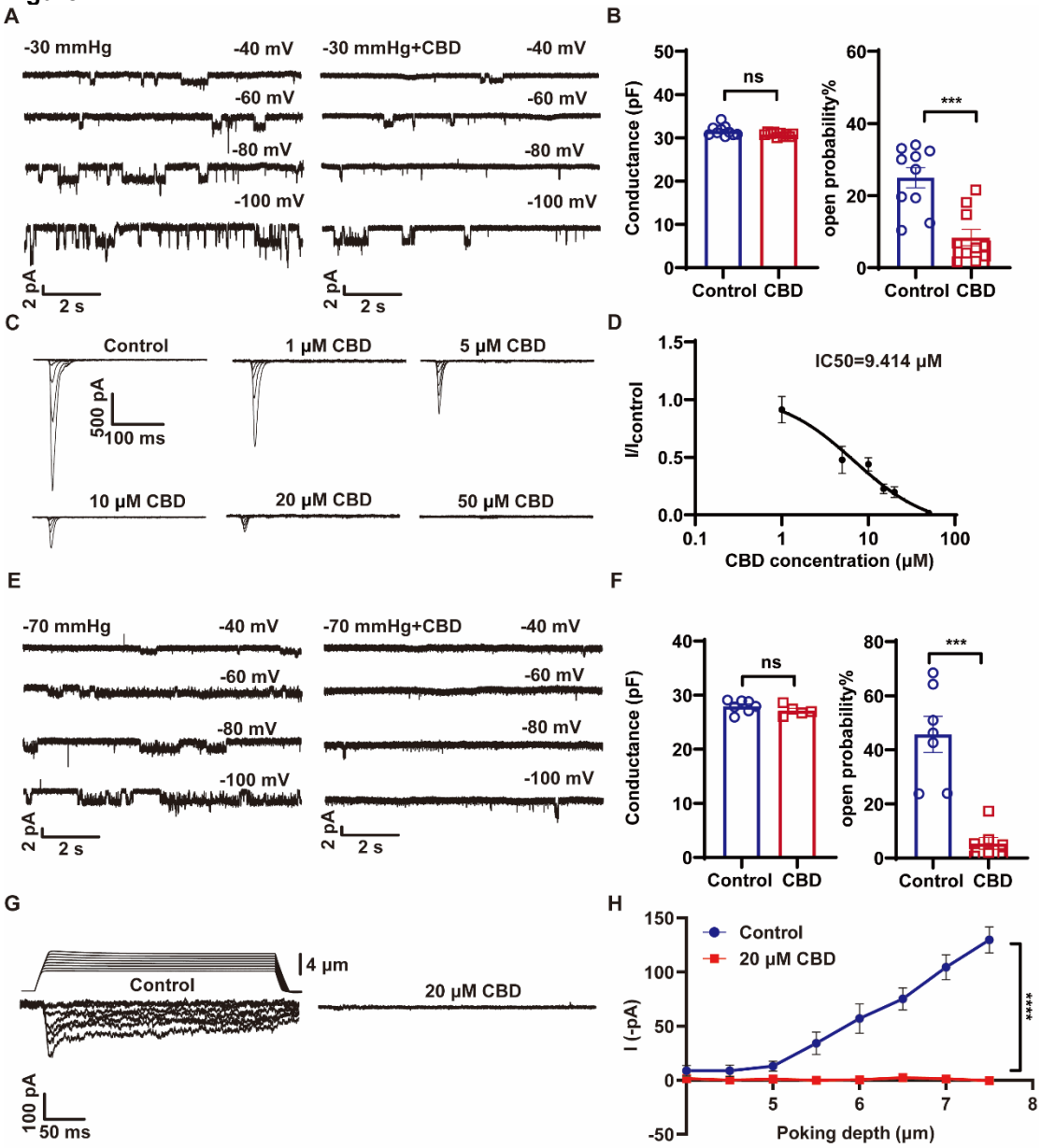

Fig. 2. CBD inhibits the function of Piezo1 channels. (*A*), Representative single-channel currents showing PIEZO1 inhibition by 20 μM CBD (right) compared to control (left) in PIEZO1-overexpressing HEK293T cells. Voltage was stepped from -100 mV to -40 mV from a holding potential of -60 mV. (*B*), Single-channel conductance (left panel) and open probability (right panel) measurements in PIEZO1-overexpressing HEK293T cells under control conditions and following CBD treatment. CBD significantly reduces the open probability of PIEZO1 without affecting conductance. (n = 10 cells, *** P < 0.001, Students unpaired t-test; mean ± SEM). (*C*), Dose-response inhibition of PIEZO1 currents by CBD. Currents recorded from PIEZO1-overexpressing HEK293T cells treated with the indicated CBD concentrations. (*D*), IC50 curve for CBD inhibition of PIEZO1 currents in transfected HEK293T cells. Currents normalized to vehicle control. (n = 7 each contraction, IC50 = 9.414 μM). (*E*), Representative single-channel recordings before and after treatment with CBD (20 μM) during negative pressure stimulation (-70 mmHg) at indicated membrane potentials (holding potential = -60 mV) in HUSMCs. CBD abolishes mechanosensitive

493 currents in HUSMCs. (*F*), Single-channel conductance (left panel) and open probability (right panel)
494 measurements in HUSMCs under control conditions and following CBD treatment. CBD
495 significantly reduces PIEZO1 open probability without affecting conductance. (*n* = 7 control; *n* = 7
496 CBD; *** *P* < 0.001, Students unpaired *t*-test; mean ± SEM). (*G*), The mechanically-activated whole-
497 cell currents were inhibited by 20 μM CBD in HUSMCs. Mechanical stimulation (4.0 ∆+ 0.5 μm
498 indentation for 300 ms) was delivered from a holding potential of -80 mV. (*H*), Poking depth-
499 response curves showing dose-dependent responses in control but not CBD-treated cells. (Control
500 and 20 μM CBD group, *n* = 10, *P* < 0.0001, two-way ANOVA; mean ± SEM).
501
502

Figure 3

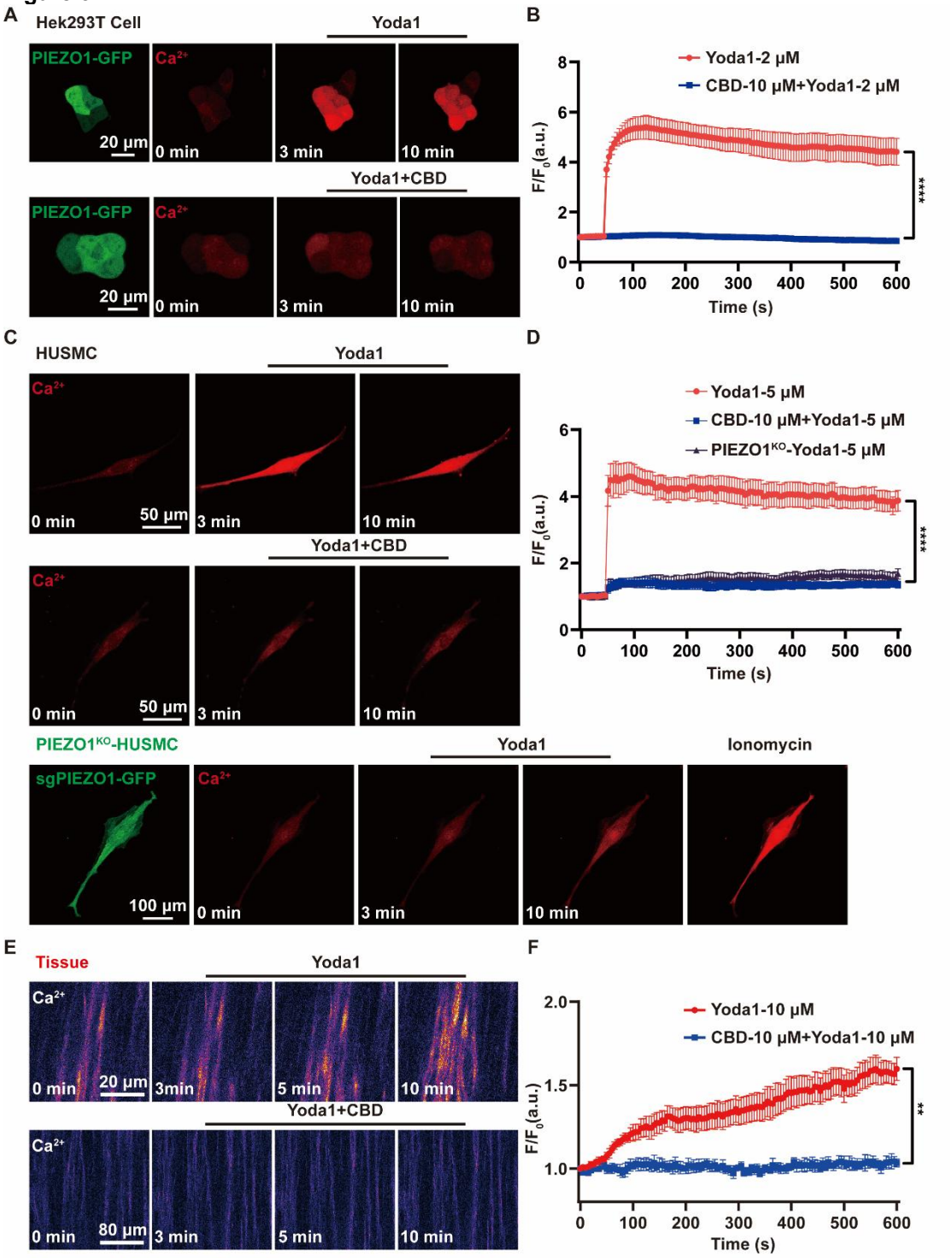

Fig. 3. Cannabidiol (CBD) suppresses PIEZO1-dependent Ca^{2+} entry in myometrial smooth muscle. (*A*), Live-cell fluorescence imaging of HEK293T cells expressing PIEZO1-GFP (green) and loaded with Ca^{2+} indicator (red). Yoda1 (2 μM) induced robust Ca^{2+} influx, which was attenuated by co-treatment with CBD (10 μM). Scale bar, 20 μm. All traces/images in (*A*) are representative of at least three independent experiments. (*B*), Quantification of Ca^{2+} responses (F/F_0) in

overexpressing PIEZO1-GFP HEK293T cells. Yoda1 (2 μM) evoked rapid Ca^{2+} influx (red, *n* = 8) that was abolished by CBD co-treatment (blue, *n* = 8). **** *P* < 0.0001, two-way ANOVA, mean ± SEM. (*C*), Live-cell fluorescence imaging of intracellular Ca^{2+} in HUSMCs. Yoda1 (5 μM) induced time-dependent Ca^{2+} influx (red) that was inhibited by co-treatment with CBD (10 μM). PIEZO1-knockout cells (sgPIEZO1-GFP, green) showed no response to Yoda1, confirming PIEZO1 specificity. Ionomycin, positive control. Scale bar, 50 μm. All traces/images in (*C*) are representative of at least three independent experiments. (*D*), Quantification of Ca^{2+} response curves in HUSMCs following Yoda1 (5 μM) treatment: significant elevation in wild-type cells (red curve, *n* = 8) that was suppressed by CBD (10 μM, blue curve, *n* = 9), while PIEZO1-knockout cells showed no response (brown curve, *n* = 8). **** *P* < 0.0001, two-way ANOVA, mean ± SEM. (*E*), Two-photon fluorescence microscopy of mouse uterine tissue showing intracellular Ca^{2+} responses. Yoda1 (10 μM) increases Ca^{2+} levels, which are suppressed by co-treatment with CBD (10 μM). (Scale bar: 40 μm). All traces/images in (*E*) are representative of at least three independent experiments. (*F*), Quantification of intracellular Ca^{2+} responses in mouse uterine tissue. Yoda1 (10 μM) significantly increased Ca^{2+} levels (red, *n* = 6), which was suppressed by CBD (10 μM, blue, *n* = 3). Images acquired at 5-second intervals for ≥10 minutes. ** *P* = 0.0064, two-way ANOVA, mean ± SEM.

Figure 4

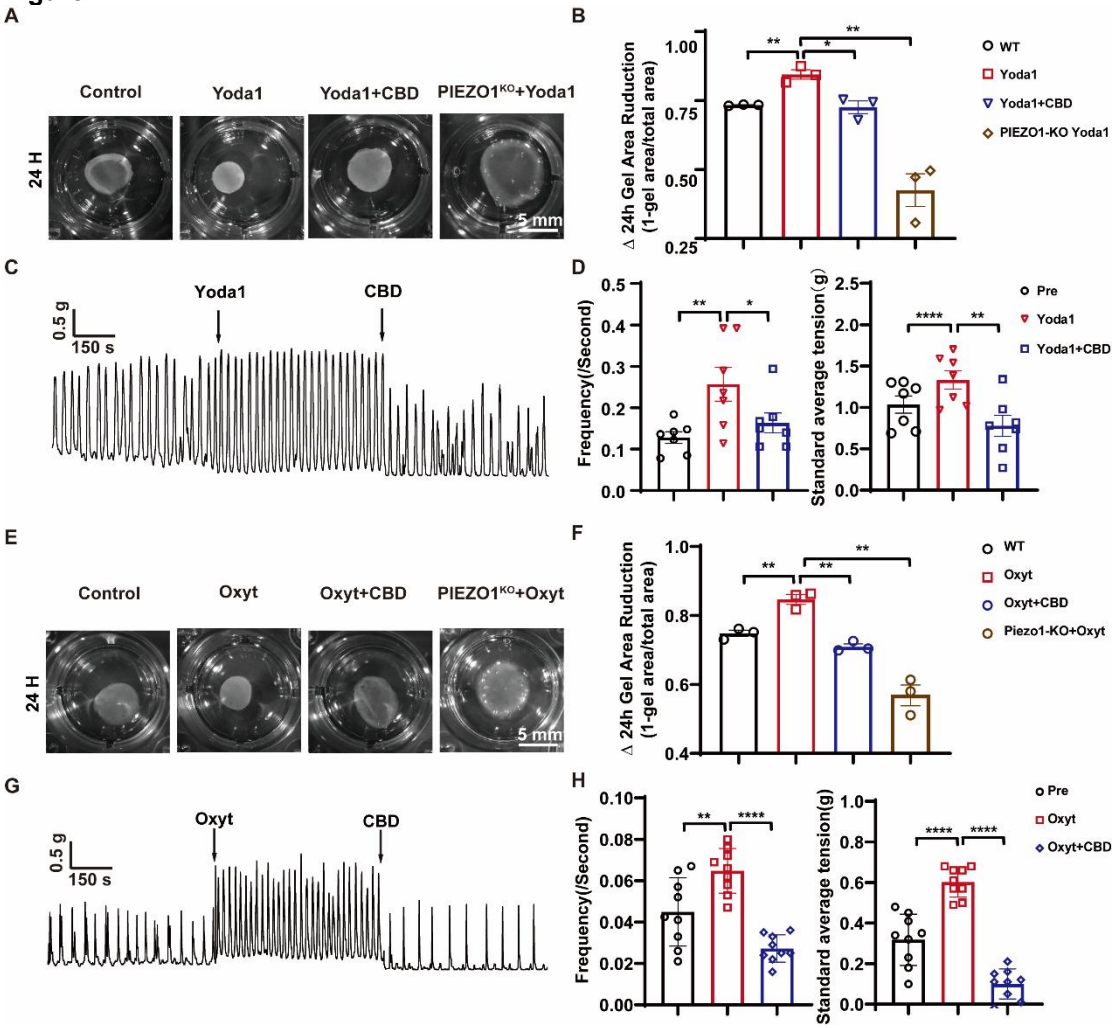

Fig. 4. CBD inhibits PIEZO1-dependent uterine contraction. (*A* and *B*), Collagen gel contraction assays after 24 h treatment. Representative images (*A*) and quantification of gel area (*B*) show control, Yoda1 (5 μM), Yoda1 (5 μM) + CBD (5 μM), and Yoda1 (5 μM) + Piezo1^{KO} HUSMC conditions. Scale bar, 5 mm. Data representative of three independent experiments. (*n* = 3 independent experiments, ns $P > 0.05$, * $P < 0.05$, ** $P < 0.01$, Students unpaired *t*-test; mean ± SEM). (*C*), Representative traces of spontaneous uterine contractions from isolated mouse uterus following treatment with 3 μM Yoda1 and 5 μM CBD. CBD markedly inhibited contractile activity. Potassium channels were blocked with 20 mM tetraethylammonium (TEA). Recordings were maintained for ≥ 10 min per segment. Data representative of three independent experiments. (*D*), Quantification of contractile frequency and normalized mean tension showing Yoda1-induced increase and subsequent CBD-mediated inhibition. Data quantified from experiments in (*C*). (*n* = 7, * $P<0.1$, ** $P<0.01$, **** $P<0.0001$, Students paired *t*-test; mean ± SEM). (*E* and *F*), Representative images (*E*) and quantification of gel area (*F*) of collagen gel contraction after 24 h treatment under the indicated conditions: control, oxytocin (2 nM), oxytocin (2 nM) + CBD (5 μM), and oxytocin (2 nM) + Piezo1^{KO} HUSMC. Scale bar, 5 mm. Images representative of three independent experiments. (*n* = 3 independent experiments; **$P < 0.01$, unpaired *t*-test; mean ± SEM.) (*G*), Representative traces of spontaneous uterine contractions from an isolated mouse uterus following treatment with 2 nM oxytocin, followed by 5 μM CBD. CBD markedly inhibited contractile activity. Recordings were maintained for ≥ 10 min per segment. Data representative of three independent experiments. (*H*), Quantification of contractile frequency and standardized mean

contractile tension showing Oxytocin-induced increase and subsequent CBD-mediated inhibition. Data quantified from experiments in (*G*). (*n* = 9, ** *P* < 0.01, **** *P* < 0.0001, Students paired *t*-test; mean ± SEM).

Figure 5

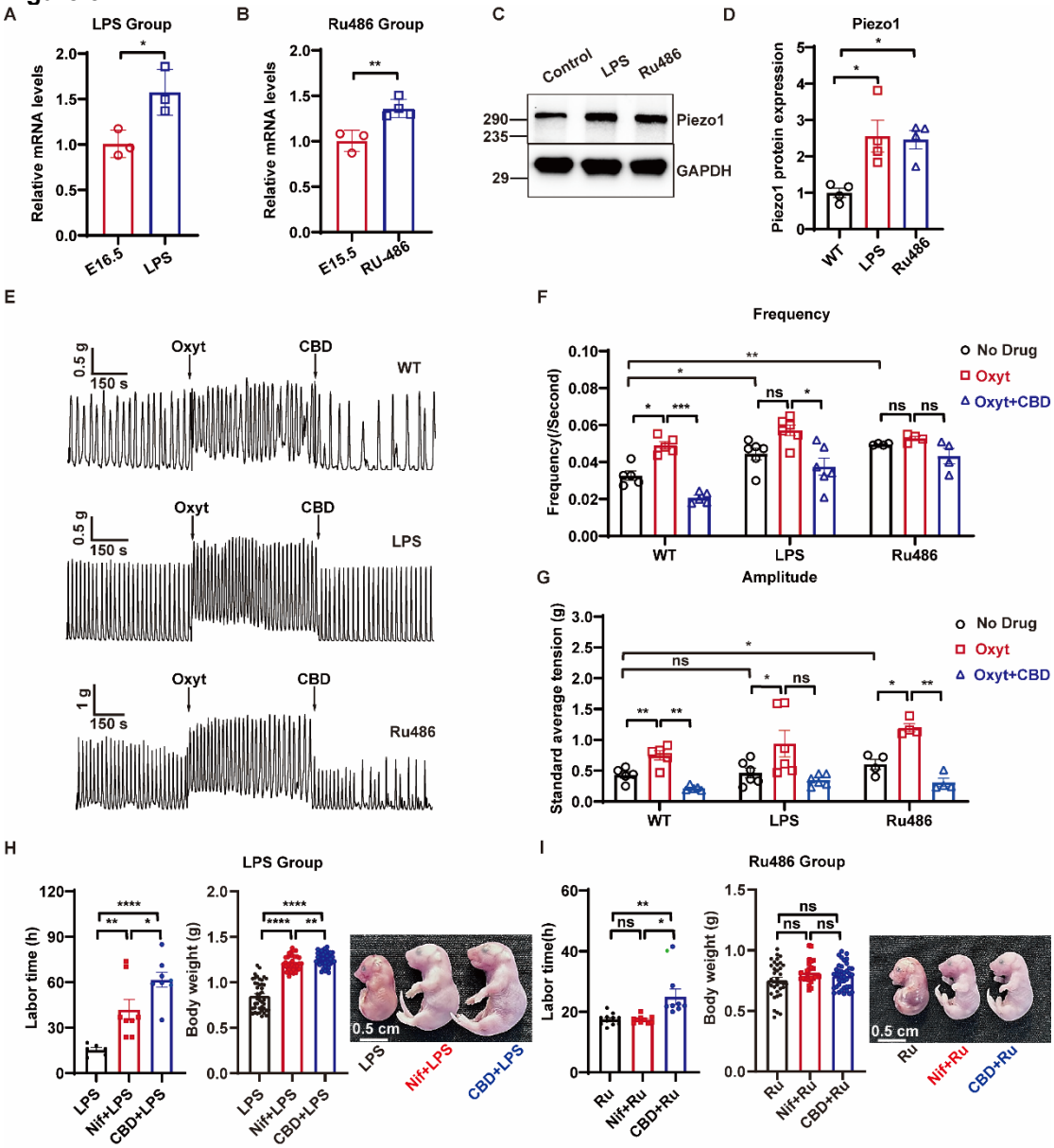

Fig. 5. CBD delays preterm labor and improves pregnancy outcomes. (*A*), Piezo1 mRNA expression is upregulated in uterine tissue from mice with LPS-induced preterm birth (100 μg/kg) compared to controls. *n* = 3 mice/group. * *P* < 0.05, Students unpaired *t*-test; mean ± SEM. (*B*), Piezo1 mRNA expression is upregulated in uterine tissue from mice with RU486 (progesterone antagonist, 150 μg)-induced preterm birth model compared to controls. Control group *n* = 3 mice, Ru486 group *n* = 4 mice. ** *P* < 0.01, Students unpaired *t*-test; mean ± SEM. (*C* and *D*), Western blot images (*C*) and quantification (*D*) of Piezo1 protein expression in uterine tissues from control, LPS-treated, and RU486-treated groups. Both LPS and RU486 treatment increased Piezo1 expression compared to control. GAPDH was used as loading control. *n* = 4, * *P* < 0.05, Students unpaired *t*-test; mean ± SEM. (*E*), Isolated uterine contractions from mice pretreated with LPS (100 μg /kg, i.p.) or RU486 (150 μg, i.p.) and stimulated with oxytocin (2 nM), followed by CBD (5 μM). Traces represent 10-minute recordings. n ≥ 3 independent experiments. All traces in (*E*) are representative of at least three independent experiments. (*F* and *G*), Quantification of contractile

570 frequency (*F*) and standardized mean contractile tension (*G*). LPS treatment increased contractile
571 frequency compared to control, whereas Ru486 had no effect. Both LPS and Ru486 treatments
572 increased mean tension relative to control. Control group *n* = 5 mice, LPS group *n* = 6 mice, Ru486
573 group *n* = 4 mice. ns *P* > 0.05, * *P* < 0.05, ** *P* < 0.01, Students unpaired *t*-test; mean ± SEM. (*H*),
574 Labor duration and pup body weight following LPS-induced preterm birth (100 μg/kg). CBD
575 treatment (20 mg/kg) significantly prolonged the delivery time and pup body weight compared to
576 the control. Nifedipine (Nif, 5 mg/kg) served as a clinical reference. Representative images of pups
577 from each treatment group (right). LPS group *n* = 6 mice, 43 pups. Nif+LPS group *n* = 8 mice, 39
578 pups. CBD+LPS group *n* = 8 mice, 41 pups. * *P* < 0.05, ** *P* < 0.01, ****P*<0.0001, Students
579 unpaired *t*-test; mean ± SEM. (*I*), Labor duration and pup body weight following Ru486-induced
580 preterm birth (150 μg). CBD treatment (30 mg/kg) significantly prolonged delivery time compared
581 to control, with no effect on pup body weight. Nifedipine (Nif, 5 mg/kg) served as clinical reference.
582 Representative images of pups from each treatment group (right). Ru486 group *n* = 11 mice, 36
583 pups. Nif+ Ru486 group *n* = 10 mice, 25 pups. CBD+ Ru486 group *n* = 8 mice, 40 pups. ns *P* >
584 0.05, * *P* < 0.05, ** *P* < 0.01, Students unpaired *t*-test; mean ± SEM.
585
586